ENVIRONMENTAL RESEARCH
LETTERS

LETTER • OPEN ACCESS

Expanding number of Western US urban centers face declining summertime air quality due to enhanced wildland fire activity

To cite this article: T Y Wilmot *et al* 2021 *Environ. Res. Lett.* **16** 054036

ENVIRONMENTAL RESEARCH
LETTERS

OPEN ACCESS

RECEIVED
15 January 2021

REVISED
19 April 2021

ACCEPTED FOR PUBLICATION
19 April 2021

PUBLISHED
30 April 2021

LETTER

Expanding number of Western US urban centers face declining summertime air quality due to enhanced wildland fire activity

T Y Wilmot[1], A G Hallar[1,2,3,*], J C Lin[1] and D V Mallia[1]

[1] University of Utah, Department of Atmospheric Science, Salt Lake City, UT, United States of America
[2] Desert Research Institute, Division of Atmospheric Science, Reno, NV, United States of America
[3] Storm Peak Laboratory, Desert Research Institute, Steamboat Springs, CO, United States of America
* Author to whom any correspondence should be addressed.

E-mail: Gannet.Hallar@utah.edu

Keywords: air quality, aerosols, wildfire, wildland fire, trend analyses, Western US, hotspot

Supplementary material for this article is available online

Abstract

Combining multiple sources of information on atmospheric composition, wildland fire emissions, and fire area burned, we link decadal air quality trends in Western US urban centers with wildland fire activity during the months of August and September for the years 2000–2019. We find spatially consistent trends in extreme levels (upper quantile) of fine particulate matter ($PM_{2.5}$), organic carbon, and absorption aerosol optical depth centered on the US Pacific Northwest during the month of August. Emerging trends were also found across the Pacific Northwest, western Montana, and Wyoming in September. Furthermore, we identify potential wildfire emission 'hotspots' from trends in wildfire derived $PM_{2.5}$ emissions and burned area. The spatial correspondence between wildfire emissions hotspots and extreme air quality trends, as well as their concomitant spatial shift from August to September supports the hypothesis that wildfires are driving extreme air quality trends across the Western US. We derive further evidence of the influence of wildland fires on air quality in Western US urban centers from smoke induced $PM_{2.5}$ enhancements calculated through statistical modeling of the $PM_{2.5}$-meteorology relationship at 18 Western US cities. Our results highlight the significant risk of increased human exposure to wildfire smoke in August at these Western US population centers, while also pointing to the potential danger of emerging trends in Western US population growth, wildfire emissions, and extreme air quality in September.

1. Introduction

Atmospheric aerosols with an aerodynamic diameter of less than 2.5 μms (particulate matter ($PM_{2.5}$)) are known to cause adverse health outcomes, such as increased emergency room visits for respiratory illness [1–4] and enhanced daily mortality [5, 6]. In light of these adverse health outcomes, $PM_{2.5}$ is treated as a 'criteria pollutant' by the US Environmental Protection agency (EPA) and regulated under the Clean Air Act, with levels set by the National Ambient Air Quality Standards (NAAQS). Currently, NAAQS attainment requires annual mean and 98th percentile $PM_{2.5}$ concentrations of less than 12 and 35 μg m^{-3}, respectively, when averaged over three years.

Despite a 43% decline in national scale average $PM_{2.5}$ concentrations over the years 2000–2019 [7], trends toward increasingly extreme air quality have been identified across much of the Western US [8]. Efforts aimed at attribution of these increases in aerosol loading have indicated biomass burning as a potential culprit. Emerging trends in $PM_{2.5}$ associated with smoke have been identified in the Pacific Northwest and portions of the surrounding Western states [9]. Positive $PM_{2.5}$ trends have been associated with elevated total carbon at sites across the Western US [8], and enhanced surface $PM_{2.5}$ and aerosol optical depth [10] have been linked to fire smoke within the Colorado Front Range. Urbanization as the driver of these aerosol trends is unlikely given evidence of decreasing trends in the annual mean of $PM_{2.5}$ and organic aerosol concentrations throughout the Western US [7, 8, 11].

Investigations of wildfire activity point to Western US aerosol trends as the result of a shifting climate,

by which increasing temperatures, aridity [12], and a declining snowpack [13] promote more frequent and intense wildfires [14–16]. Linkages between aridity, fire area burned (FAB), and aerosol loading in the Intermountain West have been documented [17]. Positive trends in FAB and the number of large wildfires from 1984 to 2011 have been identified [14], and modeling under a climate change scenario of 2 °C warming by 2050 suggests that the increasing trend will persist into the future [18]. The climate change—wildfire—aerosol linkage in the Western US will expose millions of additional people to elevated $PM_{2.5}$ annually by mid-century [19], producing a corresponding increase in premature deaths attributable to fire specific $PM_{2.5}$ [20]. Furthermore, the effects of climate change will be compounded by the legacy of decades of fire suppression, further amplifying the impact of large fires [21]. The extraordinary fire season of 2020 in the Western US [22] provides vivid testament to the societal costs of this trajectory.

With the potential nexus of increasing aerosol load, enhanced fire activity, and a growing Western US population [23] in mind, we carry out analyses to build upon existing work by: (a) improving current understanding of aerosol trends by combining a multitude of atmospheric composition data—$PM_{2.5}$, organic carbon, and absorption aerosol optical depth (AAOD); organic carbon and AAOD serve as markers for biomass burning given the ability of Western US wildfire activity to explain organic carbon variability [24] and the sensitivity of AAOD to the presence of brown carbon via differential ultraviolet absorption [25]; (b) refining the temporal resolution of aerosol trends to monthly; (c) emphasizing human exposure to degraded air quality in urban centers, where the bulk of the population resides; and (d) synthesizing wildfire emissions and fire burned area with the atmospheric composition data to illustrate potential hotspot regions that are responsible for frequent human exposure to degraded air quality.

2. Methods

2.1. Data

The spatial information, temporal information, and usage of datasets included in this study are presented in table 1. Individual dataset descriptions and maps of aerosol observation sites can be found in supplementary information (SI) section S1 (available online at stacks.iop.org/ERL/16/054036/mmedia).

2.2. Statistical methods

2.2.1. City clustering

As a means of emphasizing human exposure to degraded air quality in our analysis, Ozone Monitoring Instrument (OMI) swath AAOD trends and generalized additive modeling (GAM) were applied to observations of large 'cities' in the Western US. Given that official city boundaries do not consistently subscribe to population characteristics, these cities were defined via a city clustering procedure applied to population density and population count data from NASA's Socioeconomic Data and Applications Center [29]. This procedure allows a 'city' to be defined beyond its administrative boundaries. When defining cities, the city clustering algorithm iteratively clusters grid cells meeting a threshold population density if they are within some distance (ℓ) of each other [30]. An ℓ value of 5 km was used here, as the literature suggests values between 2 and 6 km provide the best alignment between metropolitan statistical areas and city clusters [31]. A population density threshold of 1000 km^{-2} was selected via qualitative observations of returned city clusters using population density thresholds between 500 and 1200 km^{-2}. The combination of a 5 km clustering length and a threshold population density of 1000 km^{-2} (e.g. figure S3) seemed to provide the best distribution of large cities in the West when requiring the total population of a cluster exceed 200 000 people. In total, 33 large cities within the Western US were defined using this procedure.

The city clustering performed here can be recreated by applying the cca() function from the 'osc' package in R [32] to the referenced datasets. We have found that doing so recreates the clusters developed here with a maximum discrepancy in total city population of approximately 3%. City clusters will be identical for the majority of the 33 cities defined.

When applied to OMI swath AAOD data, these city clusters are used to look for intersections of the OMI swath with city polygons produced from the gridded clusters. Each OMI pixel that intersects a given city is treated as part of that cities AAOD dataset.

2.2.2. Quantile regression (QR)

To investigate the trajectory of extreme aerosol events in the Western US, QR was applied to the EPA $PM_{2.5}$ [33], Interagency Monitoring of Protected Visual Environments (IMPROVE) [34–37] $PM_{2.5}$ and organic carbon, EPA Chemical Speciation Network (CSN) organic carbon [33, 38], and OMI swath AAOD [39] datasets on a month-by-month basis. QR was applied at upper quantiles (98th and 95th) to focus our analysis on episodic extreme aerosol events, consistent with the nature of biomass burning. A reduced quantile relative to surface aerosol datasets was used for AAOD (95th) to combat data limitations from cloud screening.

QR allows trends to be fitted to the extremes of a distribution rather than the mean (linear regression) by taking advantage of asymmetric weighting during regression [40, 41]. This asymmetric weighting is in opposition to the symmetric ordinary least squares approach used for a linear regression. An added benefit of QR is that it allows for an understanding of

Table 1. A description of the data products used. The spatial and temporal information reflects the regions and years used in this study.

Product name	Spatial info	Temporal info	Usage
EPA $PM_{2.5}$ mass (24 h)	141 sites	Daily, 2000–2019	$PM_{2.5}$ trends, GAMs inputs
IMPROVE $PM_{2.5}$ mass (24 h)	51 sites	Third day, 2000–2019	$PM_{2.5}$ trends
EPA CSN OC mass (24 h)	27 sites	Third day, 2000–2019	Organic carbon trends
IMPROVE OC mass (24 h)	96 sites	Third day, 2005–2015	Organic carbon trends
OMI swath AAOD	13 × 24 km, 33 cities	Overpass, 2005–2019	City scale AAOD trends
GPW Population Density v4.11	30 arc-sec, CONUS	2020 estimate	City clustering
GPW Population Count v4.11	30 arc-sec, CONUS	2020 estimate	City clustering
MTBS Burned Areas Boundaries	30 m, fires >405 ha, CONUS	2000–2018	Fire area burned trends
GFED 4.1s	0.25°, CONUS/CA	2000–2019	Fire $PM_{2.5}$ emission trends
MFLEI	250 m, CONUS	2003–2015	Fire $PM_{2.5}$ emission trends
QFED v2.5r1	0.1°, CONUS/CA	2000–2020	Fire $PM_{2.5}$ emission trends
FINN v1.5	1 km, CONUS/CA	2002–2019	Fire $PM_{2.5}$ emission trends
NCEP-DOE Reanalysis 2 [26]	2.5°, CONUS/CA	Daily mean, 2000–2019	GAMs inputs
Radiosonde data [27]	9 sites	00/12 UTC, 2008–2019	GAMs inputs
SPEI [28]	0.1°, CONUS	Monthly, 2008–2019	GAMs inputs
NOAA HMS Smoke Polygons	∼1 km, CONUS	Daily, 2008–2019	'Smoke' day designation

trends in the extremes of a dataset without a need to subset the data. We perform QR using the rq() function from the 'quantreg' package in R [42]. *P*-values and 95% confidence intervals were developed via a bootstrapping procedure supplied by arguments within the summ() function of the 'jtools' package [43]. Essentially, each QR was reapplied to 100 000 resampled versions of the original dataset, with replacement, to see if the regression to the actual dataset was distinguishable at $p < 0.05$ from the scatter produced by the resampled datasets. Resampled datasets were also used to construct 95% confidence intervals. Specifics of QR application to each dataset are provided in SI section S2.

2.2.3. GAM

GAMs allow for the combination of many linear or non-linear predictor variables to estimate some response variable, and have the following general form [44]:

$$g(\mu_i) = \boldsymbol{A_i\theta} + f(x1_i) + f(x2_i) + f(x3_i, x4_i)\ldots$$

where g is a link function relating the expected value of the response variable (μ_i) to a linear combination of ordinary linear model components ($\boldsymbol{A_i\theta}$) and smooth nonlinear functions (f_j) of predictor variables (x_k).

GAMs have previously been used to investigate enhancements in urban ozone resulting from wildfire smoke inundation [45, 46]. McClure and Jaffe [45] use a GAM framework to demonstrate significant increases in ozone on smoke impacted days at an EPA site in Boise, Idaho, when accounting for meteorological conditions and atmospheric transport. To achieve this, they fit a GAM to ozone concentration-meteorology/back trajectory (x_k) relationships for smoke free days and then used the model to estimate ozone concentrations on smoke impacted days (μ_i). Model estimates could be considered the expected ozone concentrations for smoke impacted days based on meteorological and transport conditions alone, meaning the model residuals (observed values—μ_i) offered an estimate of the smoke enhancements to ozone.

Here we apply a GAM framework to 18 EPA $PM_{2.5}$ monitors in the Western US to investigate the role of wildfire smoke in anomalous $PM_{2.5}$ values. EPA monitors were utilized if they fell within one of the 33 large cities defined by our city clustering procedure and possessed daily data for 2008–2019. We rely on the meteorological datasets indicated in table 1 as our predictor variables (x_k) to estimate the daily averaged $PM_{2.5}$ on smoke impacted days (μ_i). We employ an identity link function, removing $g()$ from the regression equation.

For each monitor, data was first divided into 'smoke' and 'non-smoke' days following the methods of McClure and Jaffe [45]. 'Smoke' days were required to meet two criteria: (a) the daily averaged $PM_{2.5}$ had to be in excess of one standard deviation above the mean across 2008–2019, and (b) the monitor had to fall within a NOAA Hazard Mapping System (HMS) daily smoke polygon [47]. While HMS smoke polygons have previously been used to demonstrate statistical differences in $PM_{2.5}$ concentrations when smoke is present [48], their subjective basis opens the door for false-negative 'non-smoke' designations. HMS smoke polygons are developed through manual analysis of satellite visible imagery, meaning they are subject to the obscuring effects of clouds and haze, and are best considered as a conservative estimate of smoke extent [49].

Once divided into 'smoke' and 'non-smoke' datasets, each GAM was trained on 'non-smoke' data, fitting the model based on $PM_{2.5}$-meteorology relationships, and then applied to 'smoke' data. Training on 'non-smoke' data provided a baseline from which to predict 'smoke' day $PM_{2.5}$ from meteorology alone, allowing for an estimate of the $PM_{2.5}$ enhancement due to the presence of smoke on these days. Residuals for each dataset, 'smoke' and 'non-smoke', were analyzed for statistical differences. It should be noted that the conservative nature of the 'smoke' day designation may provide for attribution of smoke driven $PM_{2.5}$ enhancements to meteorological variables within the models, resulting in a tempered estimate of typical $PM_{2.5}$ enhancements due to smoke for cities in the Western US. False negatives may also be responsible for reduced r-squared values in some GAM setups.

Specifics of GAM construction and cross-validation within R may be found in SI section S3. Table S1 describes the implementation of individual variables in each of our 18 GAMs.

2.2.4. Identification of potential emissions hotspots

Recognition of potential wildfire emissions hotspots with relevance to human exposure to poor air quality was based on linear trend analyses of monthly aggregated FAB and wildfire emitted $PM_{2.5}$ in Western US and Western Canadian ecoregions/ecoprovinces [50, 51]. Supporting statistics were generated via bootstrapping as outlined in the QR methods. Given the uncertainty in fire emissions inventories, numerous inventories were considered, including: the Monitoring Trends in Burn Severity (MTBS) [52] FAB dataset, Global Fire Emissions Database (GFED) [53–55], Fire Inventory from NCAR (FINN) [56], and Quick Fire Emissions Dataset (QFED) [57]. When possible, trends were calculated for time series ending in 2018 (a particularly active fire year) and 2019 (a rather quiet fire year) as a means of considering the sensitivity of results to emissions in the terminal year. Ecoregions/ecoprovinces demonstrating positive and statistically significant trends ($p < 0.1$, often $p < 0.05$) in FAB/$PM_{2.5}$ emissions across many inventories and time series were considered potential wildfire emissions hotspots.

FAB within the MTBS was calculated from the associated fire perimeter shapefiles using R. This calculation is to account for unburned islands within the maximum fire extent reported by MTBS. As a caveat, it should be noted that MTBS trends reflect FAB by ignition month, such that the associated emissions may occur in subsequent months. Given this, the relevant MTBS trend for the Central California Foothills and Coastal Mountains ecoregion reported here is for July (table S2).

3. Results and discussion

3.1. Western US air quality trends

QR (see section 2) analyses of $PM_{2.5}$, organic carbon, and AAOD datasets indicate statistically significant trends toward increasingly extreme air quality across large portions of the Western US, particularly during the months of August and September. Multi-year trends for August highlight the Pacific Northwest and portions of the Central California Valley as regions experiencing clear degradation of air quality, while trends in September point to the Pacific Northwest, and portions of Western Montana and Wyoming (figure 1). The consistency of spatial patterns across datasets suggests wildfires are driving trends in extreme air quality across the Western US. These findings are particularly true in urban centers, as the EPA monitor sites used for $PM_{2.5}$ analyses tend to cluster in urban settings, and our city-clustered AAOD (described within section 2) focuses on locations with elevated population density (>1000 km^{-2}) and total population (>200 000). The consistency between nearby EPA (primarily urban) and IMPROVE (primarily rural) $PM_{2.5}$ trends counters the hypothesis that these results are driven by urban development.

3.1.1. August

Figures 1(a)–(c) depict the upper quantile trends for the month of August for $PM_{2.5}$ observations from the EPA and IMPROVE networks, organic carbon observations from the EPA CSN and IMPROVE networks, and satellite-based AAOD from the OMI swath-level data, respectively. From these panels, it is apparent that the Pacific Northwest and portions of the Central California Valley are experiencing intense degradation of air quality during August. Trends in the Pacific Northwest appear especially robust in terms of spatial consistency, with many of the strongest trends in each dataset found within the states of Washington, Oregon, and Idaho. Further, a linear fit to August mean daily $PM_{2.5}$ values (figure 2) indicates that the spatial coherence in trends persists beyond the extremes (98th quantile, figure 1(d)), underscoring the severity

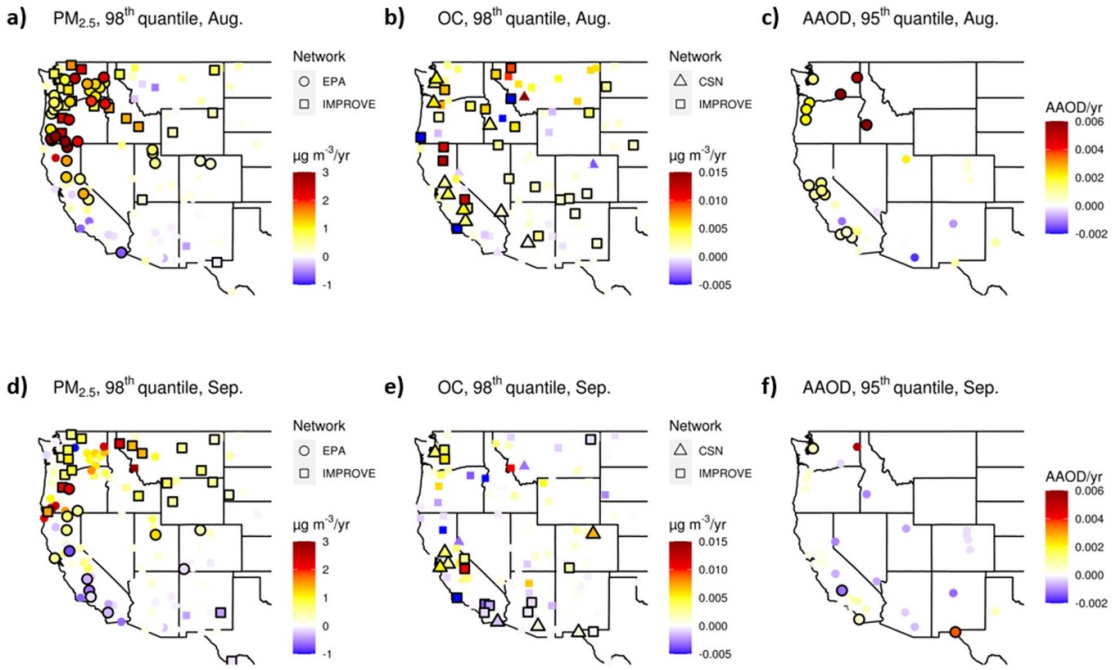

Figure 1. (a) Results of 98th quantile QR analysis for EPA (circles) and IMPROVE network (squares) $PM_{2.5}$ trends in the month of August (years: 2000–2019). Points outlined in black indicate statistical significance at $p < 0.05$. (b) Results of 98th quantile QR analysis for CSN (triangles) and IMPROVE network (squares) organic carbon trends in the month of August. CSN trends span at least 2009–2018 while IMPROVE trends span 2005–2015. Points outlined in black indicate statistical significance at $p < 0.05$. (c) Results of 95th quantile QR analysis for city-clustered OMI swath AAOD trends in the month of August spanning the years 2005–2019. Points outlined in black indicate statistical significance at $p < 0.05$. (d)–(f) Same as (a)–(c) but for September. $PM_{2.5}$ trends for additional months can be found in figures S4–S10 in SI section S4.

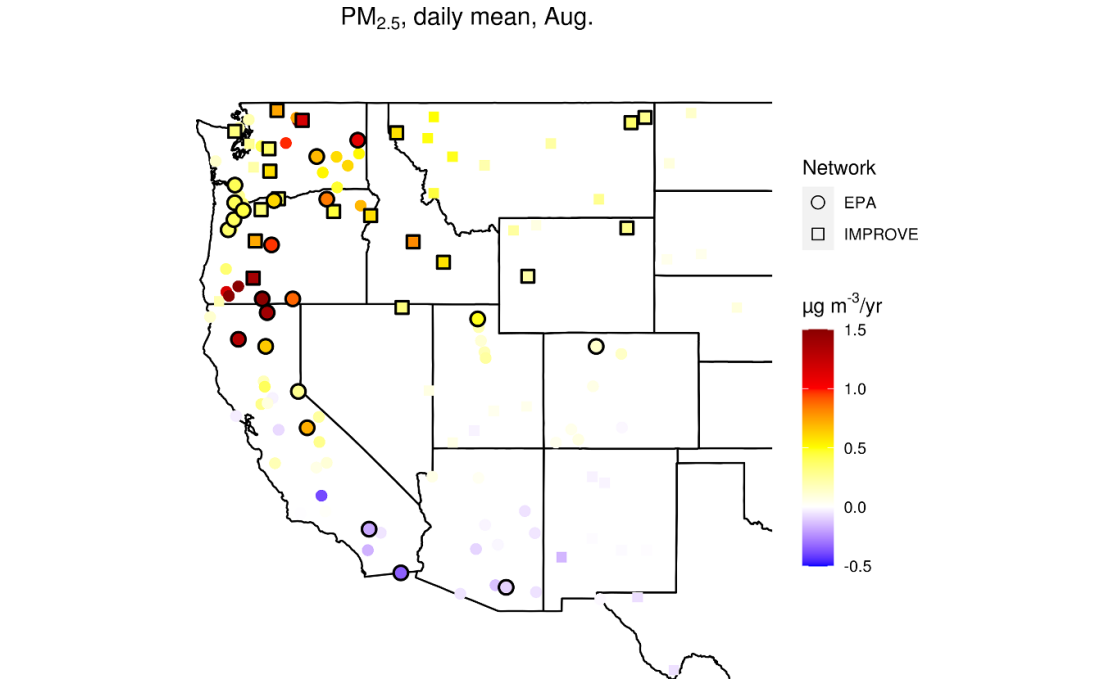

Figure 2. Results of linear trend analysis for EPA network $PM_{2.5}$ trends in the month of August (2000–2019). Points outlined in black indicate statistical significance at $p < 0.05$.

of air quality degradation in average conditions during August in the Pacific Northwest.

Overlap of positive and statistically significant trends in organic carbon and AAOD datasets with positive and significant trends in $PM_{2.5}$ strongly suggests that the $PM_{2.5}$ trends may be fire driven. However, it should be noted that areas lacking agreement across datasets may partially arise from spatial

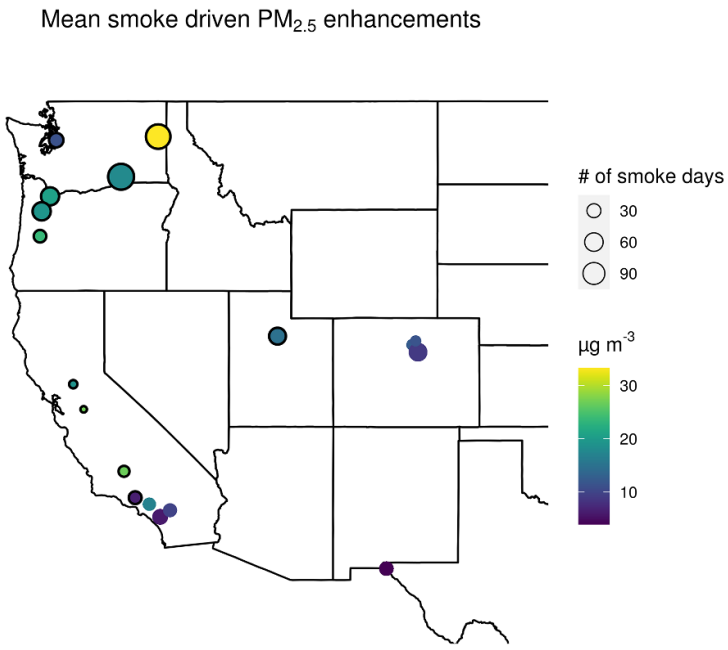

Figure 3. Mean $PM_{2.5}$ enhancements on smoke impacted days at 18 Western US EPA monitor sites (2008–2019). $PM_{2.5}$ enhancements were calculated as the model residuals on smoke impacted days when using generalized additive modeling (GAM) of the meteorology-$PM_{2.5}$ relationship. GAMs were trained on meteorology and $PM_{2.5}$ for non-smoke impacted days. Points outlined in black indicate GAM *r*-squared values in excess of 0.5. Point size reflects the number of smoke impacted days considered during GAM analysis for a given site.

under-sampling (figure S1) and/or the complexities associated with smoke transport in complex terrain and the wildfire plume rise. Plume rise may decouple surface ($PM_{2.5}$ and organic carbon) and column (AAOD) trends. Further evidence of a wildfire source is drawn from the maxima in trends of $PM_{2.5}$ and organic carbon located within or just east of the fire prone Klamath Mountains/California High North Coast Range. As detailed in later sections, the Klamath Mountains/California High North Coast Range ecoregion is characterized by increasing wildfire $PM_{2.5}$ emissions across several wildfire emissions inventories.

The presented decreasing trends in the Southwest demonstrate spatial consistency with identified trends toward reduced summertime organic aerosol concentrations [11]. Malm *et al* [11] indicate that significant decreasing summertime organic aerosol trends would prevail across the Western US were it not for outliers sourced from biomass burning.

3.1.2. September

For the month of September the 98th quantile daily $PM_{2.5}$ trends (figure 1(d)) exhibit a shift to the north and east relative to patterns in August (figure 1(a)), underscoring air quality degradation across portions of the Pacific Northwest, Western Montana, and Wyoming. Attribution of these trends to wildfires via aerosol observations is hindered by their reduced statistical significance and limited overlap with positive and significant organic carbon and AAOD trends, limited to the Seattle area. We suspect that the reduced spatial overlap of statistically significant trends, relative to August, is an artifact of the fire season maximizing in August (figure S11). For this reason, should the trends toward enhanced wildfire activity persist into the future, we expect September air quality trends to exhibit greater clarity given additional years of data. As an alternative hypothesis, increasing trends (2000–2014, $p > 0.1$) in average fine mode ($PM_{2.5}$) dust concentrations during the fall (September, October, November) suggest the potential role of dust in September aerosol trends at sites in Northwestern Montana and Western Oregon [58]. It should be noted that the reduced spatial consistency of $PM_{2.5}$ trends relative to August results, particularly in and around the Rocky Mountains, is largely the result of variable EPA/IMPROVE monitor site density (figure S1).

3.2. Smoke-driven $PM_{2.5}$ enhancements in urban centers

Clear enhancements in $PM_{2.5}$ levels on smoke impacted days in Western US urban centers are identified on the basis of GAM [37]. Mean $PM_{2.5}$ enhancements (figure 3) are calculated as the mean model residual (observed—GAM predicted $PM_{2.5}$) for this nonlinear statistical approach (see section 2). As such, model residuals reflect the GAMs' underprediction on 'smoke' days when only meteorological variables are used for prediction. Thus, residuals from the statistical model fitted through GAM (table S1) provide a way to quantify the additional $PM_{2.5}$ enhancement from wildfires after controlling for meteorology.

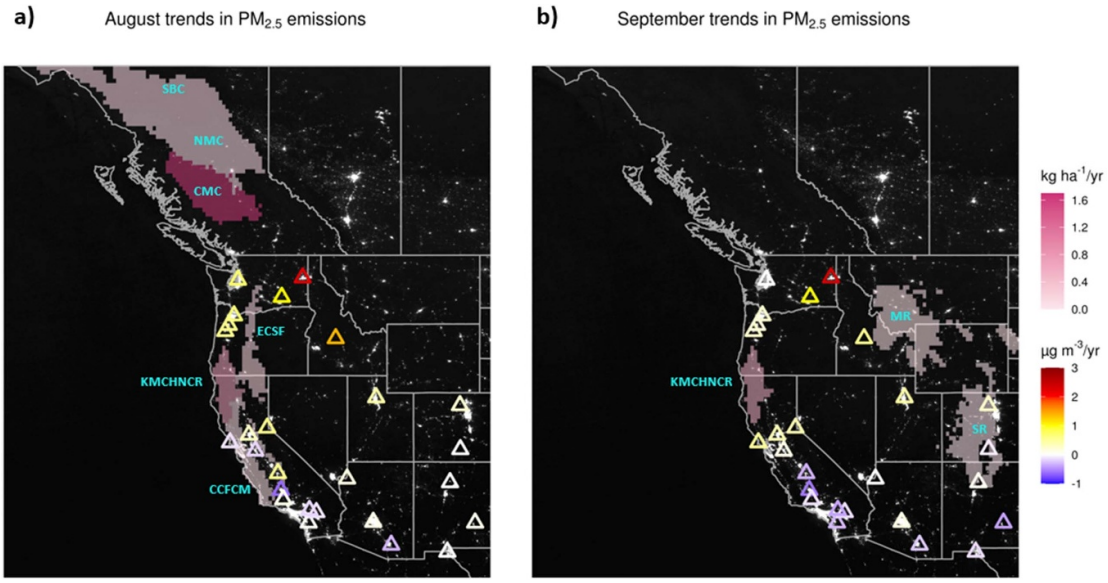

Figure 4. (a) Map of US EPA level 3 ecoregions and Canadian ecoprovinces that exhibit positive and statistically significant ($p < 0.1$) August $PM_{2.5}$ emissions trends/fire area burned trends across multiple fire emissions inventories or fire area burned products (GFED, QFED, FINN, MTBS) for timeseries ending in 2018 (a particularly active fire year) and timeseries ending in 2019 (a mild fire year). Shading is based on the area-weighted August $PM_{2.5}$ emission trend for the years 2000–2018 in the GFED inventory. For each urban center defined by our city clustering procedure, the nearest EPA monitor site with 15+ years of data is depicted as a triangle and colored according to the 98th quantile $PM_{2.5}$ trend for the month of August at that site. Background shading reflects average nighttime lights as seen by satellite for the year 2010 [59]. (b) Same as (a) but for September. Ecoregion/ecoprovince abbreviations are as follows: Southern Boreal Cordillera (SBC), Northern Montane Cordillera (NMC), Central Montane Cordillera (CMC), Eastern Cascades Slopes and Foothills (ECSF), Klamath Mountains and California High North Coast Range (KMCHNCR), Central California Foothills and Coastal Mountains (CCFCM), Middle Rockies (MR), and Southern Rockies (SR). The results of trend analyses for individual emissions inventories may be found in figures S12–S15 in SI section 6. The results of trend analyses for April–July and October–December are presented in figures S16–S28 in SI section 6.

Though applied to data for all months, our GAM results are generally in line with results from trend analyses of upper quantile air quality measures for the months of August and September. Much like the August trends, the largest mean $PM_{2.5}$ enhancements on smoke-impacted days can be found in the Pacific Northwest and California's Central Valley. Mean smoke-impacted $PM_{2.5}$ enhancements in these regions range from 18 μg m^{-3} to 33 μg m^{-3} at the Spokane site. Maximum enhancements similarly highlight the Pacific Northwest, peaking at 199 μg m^{-3} at Spokane.

While interpretation and comparison between GAM results are complicated by differing model forms (table S1), variable strength of model fits, and site-specific air quality issues (SI section S5), indicators of model performance highlight general patterns within the Pacific Northwest as being of greatest confidence. GAMs developed for urban centers in Washington and Oregon typically produced smaller mean squared normalized 'non-smoke' test residuals, possessed larger r-squared values, and were applied to a greater number of smoke impacted days, relative to GAMs developed for sites in other states. The mean and standard deviation of GAM r-squared values for sites in the Pacific Northwest were 0.61 and 0.10, respectively, as compared to 0.54 and 0.10 when considering all 18 sites. These attributes, paired with consistently larger mean enhancements relative to other regions, support the idea that urban centers in the Pacific Northwest are being subjected to especially pronounced degradation of air quality as a result of wildfire smoke.

Despite uncertainty in the exact magnitudes of GAM produced smoke driven $PM_{2.5}$ enhancements, the conservative nature, stemming from the 'smoke' day criterion (see section 2), and general sign of this analysis support the idea that wildfires are contributing to human exposure to extreme air quality in urban centers across West.

3.3. Potential wildfire emissions hotspots

Trends in monthly aggregated FAB and wildfire emitted $PM_{2.5}$ (section 2) across multiple fire emissions inventories produce a picture of wildfire activity (figure 4) that reflects the spatiotemporal evolution of trends in extreme air quality (figure 1), supporting the notion that wildfires are driving trends in extreme air quality across the Western US. Statistically significant and increasing trends in $PM_{2.5}$ and wildfire activity shift from the Pacific Northwest and the Central California Valley toward the Rocky Mountains from August to September. In August, the Pacific Northwest is uniquely situated between potential wildfire emissions hotspots in British Columbia and the Pacific Northwest/California, while also demonstrating the most extreme trends in upper quantile air

quality. Progressing into September, trends in wildfire activity relax in British Columbia and Washington, while reflecting potential emissions hotspots in Northern California/Southern Oregon and the Rocky Mountains. Similarly, September air quality trends show an attenuation relative to August in the Pacific Northwest while increasing in extent near the Rockies.

In terms of human exposure to wildfire degraded air quality, this setup highlights the colocation of August trends and Western US population centers as being of particular concern (figure 4), while also pointing to the danger of concurrent trends in Western US population growth, wildfire emissions, and extreme air quality in September. Potential explanations for the spatial differences in the seasonality of wildfire trends arise from the complex interconnections between drought and aridity, surface and canopy fuels, temporal variability of wildfire-climate relationships, and variability of historic forest management practices, across local to regional scales [60].

In the context of the wildland–urban interface (WUI), where structures intermingle with wildland vegetation and human ignitions of wildfires are common [61], the risk posed by this setup is bolstered. Recent decades are characterized by an expansion of WUI across the Western US, with growth rates by area >75% in the Northern Rockies and portions of many Western states [61]. Further, the Western US counties with the greatest potential for WUI expansion (by area) are in Southwestern Oregon and Northern California, as well as the Northern Rockies, encompassing a suspected wildfire emissions hotspot and existing in relatively close proximity to Pacific Northwest urban centers, respectively [62]. The potential for WUI expansion to exacerbate the trends identified here is cause for concern with regards to the trajectory of regional air quality in the Western US.

3.3.1. August

Results of August fire emitted $PM_{2.5}$/FAB trend analyses are dominated by trends toward elevated wildfire activity in potential hotspots in British Columbia and the mountainous Pacific Northwest/California (figure 4(a), table S2). For time series ending in 2018 (a particularly active fire year), the ecoregions/ecoprovinces comprising these potential hotspot locations demonstrate statistically significant ($p < 0.1$) results across four databases (GFED, QFED, FINN, and MTBS). Among these ecoregions/ecoprovinces, the Montane Cordillera and Klamath Mountains/California High North Coast Range stand out, with each possessing a trend of approximately 10^6 kg $PM_{2.5}$/year according to GFED emissions for 2000–2018. All trends through 2019 (a rather quiet fire year) demonstrate reduced magnitudes and weaker p-values, highlighting the sensitivity of results to the terminal year of the time series. However, each region identified in figure 4(a) has a significant trend in one or more inventories through 2019. In light of the record-breaking 2020 fire season to date [22], it is suspected that extension of these analyses will produce a rebound in trend magnitudes and statistical significance.

3.3.2. September

Reminiscent of the spatiotemporal evolution of $PM_{2.5}$, trends in FAB and fire-emitted $PM_{2.5}$ for the month of September depict the emergence of a possible hotspot for wildfire emissions in the Rocky Mountains while emission trends seem to flatten in the Pacific Northwest/California and British Columbia (figure 4(b), table S2). September trends in FAB/wildfire emissions present overall weaker magnitudes with reduced statistical significance relative to August, much like the accompanying air quality trends.

A Rocky Mountains wildfire emission hotspot in September is supported by statistically significant trends in emitted $PM_{2.5}$ for timeseries ending in 2018 and 2019 in both the GFED and QFED inventories, as well as FAB in the Southern Rockies in the MTBS dataset. Dampening of potential hotspot activity in the Pacific Northwest/California is captured by statistically significant trends being limited to the Klamath Mountains/California High North Coast Range ecoregion, which garners statistical support from the FINN (2018 timeseries only), GFED, and QFED inventories. The magnitude of GFED trends through 2018 are of order 10^5–10^6 kg $PM_{2.5}$/year for each of these three ecoregions.

While Canadian contributions to wildfire-emitted $PM_{2.5}$ trends in the month of September appear uncertain in our analysis, a possible explanation for the attenuation of emissions trends in British Columbia is provided by the southward progression of the polar jet/mid-latitude storm tracks during the transition from summer to fall. All trends pertaining to ecoregions/ecoprovinces depicted in figure 4 are provided in table S2.

4. Conclusions

We find that summertime Western US air quality is declining while wildland fire activity is increasing. In August, EPA and IMPROVE monitor sites across the Western US indicate positive trends in 98th quantile $PM_{2.5}$, with the Pacific Northwest presenting particularly robust trends. Concurrent with August $PM_{2.5}$ trends, wildland fire emissions and FAB are increasing across portions of British Columbia, Washington, Oregon, and California, uniquely placing the Pacific Northwest between two potential emissions 'hotspots'. The notion that these August $PM_{2.5}$ trends are the result of spatially linked wildfire emissions trends is further supported by analyses of organic carbon, AAOD, and smoke-driven $PM_{2.5}$ enhancements, each of which points to the Pacific Northwest and

portions of California as being impacted by wildfire smoke and extreme air quality.

In September, the spatial coverage of positive 98th quantile $PM_{2.5}$ trends shifts north and east relative to August, demonstrating clear enhancements in Western Montana and Wyoming. At the same time, the spatial distribution of wildland fire emissions trends is reconfigured such that positive trends are apparent in the Middle and Southern Rockies while trends relax in British Columbia and Washington. The correspondence in spatial shifts between wildfire emissions hotspots and extreme air quality trends from August to September provides further support for the hypothesis that wildfires are driving extreme air quality trends across the west. While we acknowledge that air quality and wildland fire trends for the month of September are less robust than those of August, we suspect the trends could emerge with greater clarity given additional data.

Thus far, the 2020 fire season has provided an exceptionally clear indication of the cost to human wellbeing should the trends we have identified persist over the coming decades. Extrapolation of the $PM_{2.5}$ trends we have identified 15 years into the future suggests that many cities in the Western US may struggle to meet NAAQS within the next few decades. Spokane, Washington provides a particularly striking example of this concern, as $PM_{2.5}$ trends at this city indicate a >16 $\mu g\ m^{-3}$ (1.26–32.35 $\mu g\ m^{-3}$, 95% confidence interval) increase in the mean and >34 $\mu g\ m^{-3}$ (15.01–53.85 $\mu g\ m^{-3}$, 95% confidence interval) increase in the 98th quantile of daily averaged $PM_{2.5}$ for the month of August by 2035. In terms of health outcomes, it has been documented that wildfire derived $PM_{2.5}$ enhancements in excess of 37 $\mu g\ m^{-3}$ have been associated with a 7.2% increase in the risk of respiratory hospital admission across all ages [2].

While our statistical findings and previous work on the air quality—wildfire connection in the Western US [8–10, 17], are highly suggestive, it is apparent that a more sophisticated, atmospheric model-based quantitative attribution of air quality trends to wildfire sources is needed. A quantitative attribution that identifies 'hotspots' for wildfire emissions with relevance to Western US population centers may provide a means for mitigation via targeted fuel treatments and related forest management practices.

Data availability statement

All data that support the findings of this study are included within the article (and any supplementary files).

Acknowledgments

The authors are grateful to the Center for High Performance Computing at the University of Utah for computational resources. We would also like to thank the US EPA, IMPROVE network, and NASA Goddard Space Flight Center for atmospheric composition data. IMPROVE is a collaborative association of state, tribal, and federal agencies, and international partners. US Environmental Protection Agency is the primary funding source for IMPROVE, with contracting and research support from the National Park Service. The Air Quality Group at the University of California, Davis is the central analytical laboratory for IMPROVE data, with ion analysis provided by Research Triangle Institute, and carbon analysis provided by Desert Research Institute. We are thankful to NASA, the Gordon and Betty Moore Foundation, and The Netherlands Organisation for Scientific Research for funding GFED. Additionally, we are thankful to the National Center for Atmospheric Research, NASA Global Modeling and Assimilation Office, and the US Geological Survey Center for Earth Resources Observation and Science and the USDA Forest Service Geospatial Technology and Applications Center for FINN, QFED, and MTBS data, respectively. We are grateful to the NASA Socioeconomic Data and Applications Center for gridded population datasets. We appreciate the financial support of the iNterdisciplinary EXchange for Utah Science, an interdisciplinary research institute at the University of Utah.

Author contributions

Gannet Hallar and John Lin designed the study. Taylor Wilmot carried out the data analyses and generated the figures, with input from Gannet Hallar, John Lin, and Derek Mallia. Taylor Wilmot wrote the manuscript, with edits provided by Gannet Hallar, John Lin, and Derek Mallia.

ORCID iDs

T Y Wilmot https://orcid.org/0000-0002-3463-1420
A G Hallar https://orcid.org/0000-0001-9972-0056
J C Lin https://orcid.org/0000-0003-2794-184X
D V Mallia https://orcid.org/0000-0003-1983-7305

References

[1] Black C, Tesfaigzi Y, Bassein J A and Miller L A 2017 Wildfire smoke exposure and human health: significant gaps in research for a growing public health issue *Environ. Toxicol. Pharmacol.* **55** 186–95
[2] Liu J C *et al* 2017 Wildfire-specific fine particulate matter and risk of hospital admissions in urban and rural counties *Epidemiology* **28** 77–85
[3] Haikerwal A, Akram M, Sim M R, Meyer M, Abramson M J and Dennekamp M 2016 Fine particulate matter ($PM_{2.5}$) exposure during a prolonged wildfire period and emergency department visits for asthma *Respirology* **21** 88–94

[4] Delfino R J et al 2009 The relationship of respiratory and cardiovascular hospital admissions to the California wildfires of 2003 *Occup. Environ. Med.* **66** 189–97
[5] Schwartz J, Dockery D W and Neas L M 1996 Is daily mortality associated specifically with fine particles? *J. Air Waste Manage. Assoc.* **46** 927–39
[6] Xing Y-F, Xu F-H, Shi M-H and Lian Y-X 2016 The impact of $PM_{2.5}$ on the human respiratory system *J. Thorac. Dis.* **8** E69–E74
[7] US EPA 2020a Particulate matter ($PM_{2.5}$) trends [data page] (available at: www.epa.gov/air-trends/particulate-matter-pm25-trends)
[8] McClure C D and Jaffe D A 2018a US particulate matter air quality improves except in wildfire-prone areas *Proc. Natl Acad. Sci. USA* **115** 7901–6
[9] O'Dell K, Ford B, Fischer E V and Pierce J R 2019 Contribution of wildland-fire smoke to US $PM_{2.5}$ and its influence on recent trends *Environ. Sci. Technol.* **53** 1797–804
[10] Val Martin M, Heald C L, Ford B, Prenni A J and Wiedinmyer C 2013 A decadal satellite analysis of the origins and impacts of smoke in Colorado *Atmos. Chem. Phys.* **13** 7429–39
[11] Malm W C, Schichtel B A, Hand J L and Collett J L Jr 2017 Concurrent temporal and spatial trends in sulfate and organic mass concentrations measured in the IMPROVE monitoring program *J. Geophys. Res. Atmos.* **122** 10462–76
[12] Seager R et al 2007 Model projections of an imminent transition to a more arid climate in Southwestern North America *Science* **316** 1181–4
[13] Mote P W, Li S, Lettenmair D P, Xiao M and Engel R 2018 Dramatic declines in snowpack in the western US *Nat. Partner J. Clim. Atmos. Sci.* **1** 2
[14] Dennison P E, Brewer S C, Arnold J D and Moritz M A 2014 Large wildfire trends in the western United States, 1984–2011 *Geophys. Res. Lett.* **41** 2928–33
[15] Westerling A L, Hidalgo H G, Cayan D R and Swetnam T W 2006 Warming and earlier spring increase western U.S. forest wildfire activity *Science* **313** 940–3
[16] Westerling A L 2016 Increasing western US forest wildfire activity: sensitivity to changes in the timing of spring *Phil. Trans. R. Soc.* B **371** 20150178
[17] Hallar A G, Molotch N P, Hand J L, Livneh B, McCubbin I B, Peterson R, Michalsky J, Lowenthal D and Kunkel K E 2017 Impacts of increasing aridity and wildfires on aerosol loading in the intermountain Western US *Environ. Res. Lett.* **12** 14006
[18] Spracklen D V, Mickley L J, Logan J A, Hudman R C, Yevich R, Flannigan M D and Westerling A L 2009 Impacts of climate change from 2000–2050 on wildfire activity and carbonaceous aerosol concentrations in the western United States *J. Geophys. Res.* **114** D20301
[19] Liu J C, Mickley L J, Sulprizio M P, Dominici F, Yue X, Ebisu K, Anderson G B, Kahn R F A, Bravo M A and Bell M L 2016 Particulate air pollution from wildfires in the Western US under climate change *Clim. Change* **138** 655–66
[20] Ford B, Val Martin M, Zelasky S E, Fischer E V, Anenberg S C, Heald C L and Pierce J R 2018 Future fire impacts on smoke concentrations, visibility, and health in the contiguous United States *GeoHealth* **2** 229–47
[21] Mell W E, Manzello S L, Maranghides A, Butry D and Rehm R G 2010 The wildland–urban interface fire problem—current approaches and research needs *Int. J. Wildland Fire* **19** 238–51
[22] Higuera P E and Abatzoglou J T 2020 Record-setting climate enabled the extraordinary 2020 fire season in the western United States *Glob. Change Biol.* **27** 1–2
[23] U.S. Census Bureau 2012 United States Summary: 2010 [data summary] (available at: www.census.gov/prod/cen2010/cph-2-1.pdf)
[24] Spracklen D V, Logan J A, Mickley L J, Park R J, Yevich R, Westerling A L and Jaffe D A 2007 Wildfires drive interannual variability of organic carbon aerosol in the western U.S. in summer *Geophys. Res. Lett.* **34** L16816
[25] Mok J et al 2016 Impacts of brown carbon from biomass burning on surface UV and ozone photochemistry in the Amazon Basin *Sci. Rep.* **6** 36940
[26] NOAA 2020b NCEP-DOE reanalysis 2, NOAA Physical Sciences Laboratory [data set] (available at: https://psl.noaa.gov/thredds/catalog/Datasets/)
[27] Iowa Environmental Mesonet 2020 Rawinsonde (RAOB) data archive, Iowa State University [data files] (available at: https://mesonet.agron.iastate.edu/archive/raob/)
[28] Beguería S, Latorre B, Reig F and Vicente-Serrano S M 2020 Global SPEI database [database] (available at: https://spei.csic.es/database.html)
[29] Center for International Earth Science Information Network (CIESIN), Columbia University 2018 Documentation for the gridded population of the world, version 4 (GPWv4), revision 11 data sets (Palisades, NY: NASA Socioeconomic Data and Applications Center (SEDAC) (available at: 10.7927/H45Q4T5F)
[30] Rozenfeld H D, Rybski D, Andrade J S Jr, Batty M, Stanley H E and Makse H A 2008 Laws of population growth *Proc. Natl Acad. Sci. USA* **105** 18702–7
[31] Rozenfeld H D, Rybski D, Gabaix X and Makse H A 2011 The area and population of cities: new insights from a different perspective on cities *Am. Econ. Rev.* **101** 2205–25
[32] Kriewald S, Fluschnik T, Reusser D and Rybski D 2019 Osc: orthodromic spatial clustering. R package version 1.0.5 (available at: https://CRAN.R-project.org/package=osc)
[33] US EPA 2020b Air data: air quality data collected at outdoor monitors across the us [data files] (available at: www.epa.gov/outdoor-air-quality-data)
[34] Federal Land Manager Environmental Database 2020 IMPROVE aerosol [data set] (available at: http://views.cira.colostate.edu/fed/QueryWizard/)
[35] Chow J C, Watson J G, Pritchett L C, Pierson W R, Frazier C A and Purcell R G 1993 The dri thermal/optical reflectance carbon analysis system: description, evaluation and applications in U.S. air quality studies *Atmos. Environ.* A **27** 1185–201
[36] Malm W C, Sisler J F, Huffman D, Eldred R A and Cahill T A 1994 Spatial and seasonal trends in particle concentration and optical extinction in the United States *J. Geophys. Res. Atmos.* **99** 1347–70
[37] Hand J L, Prenni A J, Schichtel B A, Malm W C and Chow J C 2019 Trends in remote $PM_{2.5}$ residual mass across the United States: implications for aerosol mass reconstruction in the IMPROVE network *Atmos. Environ.* **203** 141–52
[38] US EPA 2020c Chemical speciation network (CSN) [data page] (available at: www.epa.gov/amtic/chemical-speciation-network-csn)
[39] Torres O 2018 OMI/Aura near UV aerosol index, optical depth and single scattering albedo 1-orbit L2 13×24 km [dataset] *NASA Goddard Space Flight Center, Goddard Earth Sciences Data and Information Services Center (GES DISC)*
[40] Koenker R and Bassett G Jr 1978 Regression quantiles *Econometrica* **46** 33–50
[41] Koenker R 2005 *Quantile Regression* (Cambridge: Cambridge University Press)
[42] Koenker R 2020 Quantreg: quantile regression. R package version 5.75 (available at: https://CRAN.R-project.org/package=quantreg)
[43] Long J A 2020 Jtools: analysis and presentation of social scientific data. R package version 2.1.0 (available at: https://CRAN.R-project.org/package=jtools)
[44] Wood S N 2017 *Generalized Additive Models: An Introduction with R* (Boca Raton, FL: CRC Press)
[45] McClure C D and Jaffe D A 2018b Investigation of high ozone events due to wildfire smoke in an urban area *Atmos. Environ.* **194** 146–57
[46] Gong X, Kaulfus A, Nair U and Jaffe D A 2017 Quantifying O_3 impacts in urban areas due to wildfires using a

generalized additive model *Environ. Sci. Technol.* **51** 13216–23
[47] NOAA 2020c Hazard mapping system fire and smoke product, NOAA office of satellite and product operations [dataset] (available at: www.ospo.noaa.gov/Products/land/hms.html)
[48] Kaulfus A S, Nair U, Jaffe D A, Christopher S A and Goodrick S 2017 Biomass burning smoke climatology of the United States: implications for particulate matter air quality *Environ. Sci. Technol.* **51** 11731–41
[49] Rolph G D *et al* 2009 Description and verification of the NOAA smoke forecasting system: the 2007 fire season *Weather Forecast.* **24** 361–78
[50] US EPA 2020d Level III and IV ecoregions of the continental united states [dataset] (available at: www.epa.gov/eco-research/level-iii-and-iv-ecoregions-continental-united-states)
[51] Government of Canada 2020 Terrestrial ecoprovinces of Canada [dataset] (available at: https://open.canada.ca/data/en/dataset/98fa7335-fbfe-4289-9a0e-d6bf3874b424)
[52] Eidenshink J, Schwind B, Brewer K, Zhu Z-L, Quayle B and Howard S 2007 A project for monitoring trends in burn severity *Fire Ecol. Spec. Issue* **3** 3–21
[53] van der Werf G R *et al* 2017 Global fire emissions estimates during 1997–2016 *Earth Syst. Sci. Data* **9** 697–720
[54] Giglio L, Randerson J T and van der Werf G R 2013 Analysis of daily, monthly, and annual burned area using the fourth-generation global fire emissions database (GFED4) *J. Geophys. Res.* **118** 317–28
[55] Randerson J T, Chen Y, van der Werf G R, Rogers B M and Morton D C 2012 Global burned area and biomass burning emissions from small fires *J. Geophys. Res.* **117** G04012
[56] Wiedinmyer C, Akagi S K, Yokelson R J, Emmons L K, Al-Saadi J A, Orlando J J and Soja A J 2011 The Fire INventory from NCAR (FINN): a high resolution global model to estimate the emissions from open burning *Geosci. Model Dev.* **4** 625–41
[57] Darmenov A and da Silva A M 2013 The quick fire emissions dataset (QFED) documentation of versions 2.1, 2.2 and 2.4, ed R D Koster *NASA TM*-2013-104606 vol 32 p 183
[58] Hand J L, Gill T E and Schichtel B A 2017 Spatial and seasonal variability in fine mineral dust and coarse aerosol mass at remote sites across the United States *J. Geophys. Res. Atmos.* **122** 3080–97
[59] NOAA 2020a Nighttime Lights Time Series Version 4, Defense Meteorological Program Operational Linescan System, Earth Observation Group, Payne Institute for Public Policy, Colorado School of Mines [data set] (available at: https://developers.google.com/earth-engine/datasets/catalog/NOAA_DMSP-OLS_NIGHTTIME_LIGHTS#description)
[60] Littell J S, Peterson D L, Riley K L, Liu Y and Luce C H 2016 A review of the relationships between drought and forest fire in the United States *Glob. Change Biol.* **22** 2353–69
[61] Radeloff V C *et al* 2018 Rapid growth of the US wildland–urban interface raises wildfire risk *Proc. Natl Acad. Sci. USA* **115** 3314–9
[62] Gude P, Rasker R and van den Noort J 2008 Potential for future development on fire-prone lands *J. For.* **106** 198–205